PPPL-3152 - Preprint Date: December 1995, UC-420, 421, 427

TRANSP Simulations of ITER Plasmas

R. V. Budny, D. C. McCune, M. H. Redi, J. Schivell, and R. M. Wieland

Princeton University

Plasma Physics Laboratory

P. O. Box 451, Princeton NJ, 08543

Abstract

The TRANSP code is used to construct comprehensive, self-consistent models for ITER discharges. Plasma parameters are studied for two discharges from the ITER "Interim Design" database producing 1.5 GW fusion power with a plasma current of 21 MA and 20 toroidal field coils generating 5.7 T. Steady state profiles for T_{ion}, T_e, n_e, Z_{eff}, and P_{rad} from the database are specified. TRANSP models the full up/down asymmetric plasma boundary within the separatrix. Effects of high-energy neutral beam injection, sawteeth mixing, toroidal field ripple, and helium ash transport are included.

Results are given for the fusion rate profiles, and parameters describing effects such as alpha particle slowing down, the heating of electrons and thermal ions, and the thermalization rates. Thedeposition of 1 MeV neutral beam ions is predicted to peak near theplasma center, and the average beam ion energy is predicted to be half the injected energy. Sawtooth mixing is predicted to broaden the fast alpha profile. The toroidal ripple losses rate of alpha energy is estimated to be 3% before sawtooth crashes and to increase by a factor of three to four immediately following sawtooth crashes.

Assumptions for the thermal He transport and the He recycling coefficient at the boundary are discussed. If the ratio of helium and energy confinement times, τ^*_{He} / τ_E is less than 15, the steady state fusion power is predicted to 1.5 GW or greater. The values of the transport coefficients required for this fusion power depend on the He recycling coefficient at the separatrix. If R_{rec} is near 1, the required He diffusivity must be much larger than that measured in tokamaks. If $R_{rec} \leq 0.50$, and if the inward pinch is small, values comparable to those measured are compatible with 1.5 GW.

1. Introduction

One of the goals for ITER is the production of 1.5 GW of fusion power for long durations [1]. The required plasma conditions are far beyond those produced in current Tokamak experiments, thus considerable effort has been devoted to studying the extrapolations

of scaling laws to ITER discharges. A database of possible discharges that achieve this goal of 1.5 GW is being assembled [2].

One of the crucial issues for ITER is whether the alpha heating will be sufficient and the alpha particle losses will be tolerable. Good alpha confinement is necessary for self-sustained fusion reactions. Thermal alpha ash concentration must remain low so that the D and T will not be excessively depleted.

In order to predict alpha parameters, comprehensive modeling of ITER discharges is needed. The local transport must be sufficiently benign to achieve high densities and temperatures for the deuterium and tritium, and low concentrations of impurities. Large plasma currents need to be driven. Sawteeth and ripple effects need to be assessed.

To facilitate and focus the modeling efforts, two of the discharges in the ITER database have been selected as test beds for comparing predictive modeling codes. One discharge has flat profiles and the other has moderately peaked profiles. Various predictive codes with different strengths and weaknesses, are being used to model these discharges.

This paper describes simulations using the TRANSP plasma analysis code [3] for these two ITER discharges. Although TRANSP is not primarily a predictive code, it use offers a number of capabilities that complement the predictive codes. These capabilities are discussed in the next Section. In this paper TRANSP is used to model the high-energy neutral beam injection, sawteeth effects, toroidal field ripple effects, and helium ash concentrations. Ranges of helium ash transport that result in equilibrium ash profiles consistent with 1.5 GW of fusion power are given. The overall goal of this paper is to develop TRANSP models for ITER to complement predictive code modeling.

2. TRANSP Capabilities

TRANSP has a number of useful capabilities that make it a powerful tool for studying ITER plasma performance. These include:

General flux geometry - The geometry of the boundary (such as the 98% flux surface of diverted discharges) can be specified as a general function of time. The interior flux surfaces are computed solving the Grad-Shafranov equation. TRANSP has recently been generalized [4] to model up-down asymmetry. The boundary surface from the ITER database assumed here is designated x = 1 in Fig. 1. The interior flux surfaces are parameterized by the square-root of the normalized toroidal flux.

Multiple species - Up to five thermal ion species can be modeled in any run. The species that have been incorporated into TRANSP are H, D, T, He^3, He^4, Li, and an impurity of arbitrary Z and A. Several models for the relative transport of the H, D, and T are available. Explicit transport coefficients for the thermal He ash can be modeled.

Auxiliary heating and current drive - Effects of NBI, ICRF, and LHCD can be simulated. These capabilities allow us to compute the power deposition and the corresponding transport coefficients. The capabilities of simulating FWCD and ECH are being developed.

Detailed beam deposition - Monte Carlo techniques are used to model the beam deposition in 3D. An estimation of multi-step ionization effects is included. Injection of H, D, T, and He beams can be modeled. We discuss the effects of D-NBI in Section 4.

Non-zero orbit effects - Monte Carlo techniques are used to simulate orbits of alpha particles and beam ions. These give accurate simulations of the pressure and beam-driven currents in present Tokamak experiments. They are being used to study alpha parameters in TFTR. Either neoclassical orbits, or the possible effects of anomalous fast ion diffusion can be modeled.

Fusion Products Modeling - The slowing down and heating of the thermal plasma by the fast alpha particles is modeled. Various losses, such as those caused by orbits intercepting the vacuum vessel are modeled.

Sawteeth Effects - Models for sawteeth effects on the thermal plasma and on the fast ions have been incorporated into TRANSP [3,5]. These are useful for estimating q_ψ profiles and how much of the fast ions will be mixed. Sawteeth effects are discussed in Section 5.

Toroidal Field Ripple Loss - A model for estimating the toroidal field ripple losses of fast ions has recently been incorporated into TRANSP [6,7,8]. The number and energy of the lost ions are computed. Values of the toroidal field ripple,

$$\delta(R,z) \equiv F(B_{max} - B_{min}, B_{max} + B_{min})$$

are specified. Contours of the values from the ITER database assumed here are shown in Fig. 2. Losses are discussed in Section 6.

Fast Ion distributions - The distributions in space, energy, and pitch angle are calculated. These are useful for estimating the effects of fast ions on the MHD and TAE modes.

Coupling with MHD and TAE codes - Outputs from TRANSP runs can be used as inputs for codes such as ORBIT [9], PEST [10], and NOVA [11].

Diagnostic Simulations - TRANSP is capable of calculating various plasma profiles and chordal emissions along user-chosen chords. This is useful for designing diagnostics and for interpreting their results.

The TRANSP analysis code is being used extensively to analyze current Tokamak experimental results from TFTR [3,5,12], JET [10], PBX-M [13], TEXTOR [14], TORE SUPRA [15], and C-MOD [16]. The widespread use of TRANSP increases its reliability and

facilitates comparisons of results from different experiments. TRANSP has also been used for making predictions for future Tokamak reactor performance [17,18,19].

3. Baseline ITER Simulations

The ITER discharges are assumed to have I_p = 21 MA and 20 toroidal field coils generating B_{TF} = 5.7 T. The boundary flux surface is assumed to have an elongation of 1.6 and a triangularity of ≅ 0.25. The profiles used are those from the ITER "interim" database (c.a. April, 1995) designated 1001 with flat profiles and 1002 with peaked profiles. The n_e profiles are compared in Fig. 3. The impurity profiles are calculated using the Z_{eff} profiles from the database and a choice for the Z of the impurity. The assumed profiles for Z_{eff} are approximately 1.55, as shown in Fig. 4-a. The Z of the impurity is assumed to be 4.5 representing Be with Z = 4 and a contribution from other impurities with higher Z. The radiation profiles are also given in the database, as shown in Fig. 4-b, and are used in the TRANSP modeling for calculating the electron power balance. The temperature profiles assumed for the two categories of discharges are shown in Figs. 5.

The densities of the thermal D, T, He, impurity and of the beam ions and fast alpha particles are calculated by TRANSP. Several models are available for computing the relative D and T mixing. The model that gives the best agreement with measurements of neutron emission profiles in TFTR has a preferential inward pinch of D relative to T [21]. This model gives pessimistic results for ITER by increasing the D density at the expense of the T density. In the following we use the more optimistic model with equal transport of the D and T. Examples of profiles are compared in Figs. 6. The computed densities of the fast ions, n_{beam} and $n_{\alpha,}$ are relatively low, even compared to the density of the impurity, n_{imp}. The thermal He profile n_{He} is calculated from the thermalization rate profile and the assumed He transport. Various He transport assumptions are discussed in Section 7. The thermal He density has a significant effect on the fusion rate by depleting the D and T densities at fixed n_e. If there were no thermal He, the fusion power from the assumed profiles would be around 2.5 GW. Results for alpha parameters for two cases with P_{DT} ≅ 1.5 GW are summarized in Table I.

The steady-state phases of ITER discharges, including the periodic effects of sawteeth with a period of 50 sec, are discussed here. This relatively long sawtooth period allows the q_ψ profile a long time to relax after a sawtooth crash. A short sawtooth period is predicted to reduce the perturbations of q_ψ, as discussed in Section 5, but to enhance the ripple loss of fast alpha particles, as discussed in Section 6. Approximately 120 sec of the discharges are modeled in order to simulate several crashes of sawteeth, and to allow the thermal He to approach equilibrium. The NBI duration is limited to 50 sec in order to provide

results both with and without NBI for evaluating the effects of NBI.

4. Neutral beam injection

The current plan for ITER is to use up to 100 MW of auxiliary heating / current drive. Some or all of this power could be D or H injection from three negative ion beam sources. These sources would be situated approximately 29 m from the center line, and aimed with tangency radii of 6.5 m in the direction of the plasma current. The injected neutrals are assumed to have the full energy, which is planned to be up to 1 MeV.

The beam neutrals depositions are calculated using Monte Carlo techniques. Examples for the deposition profiles are shown in Fig. 7. The dominant deposition rate is ionization by collisions with the thermal D and T ions. The source profiles for the fusion alphas is calculated from the thermonuclear, beam- thermal, and beam-beam fusion rates. Examples of the fusion profiles are shown in Fig. 8.

The fast-ion distributions are calculated using Monte Carlo techniques. The profiles of the slowing down times for the fast ions are compared in Fig. 9. The average energy of the beam ions is approximately half the injection energy, as shown in Fig. 10. The average energy of the fusion ions is 1.5 MeV over most of the plasma profile, as shown in Fig 10. Their average energy in the edge is higher since they are lost before they have much chance to slow down. The alpha contribution to the central pressure is 10-15%. The beam ion contribution to the central pressure is ~ 2%. The beam contribution to the fusion rate ~ 1%.

TRANSP calculates the beam-ion and fast alpha distributions,

$$F(df_j(E_j,\lambda_j,x,t),dVdE_j)$$

The independent variables are the energy E_j of the fast species j, $\lambda_j \equiv v_{parallel} / v \equiv \cos(\text{pitch angle})$ with $v_{parallel}$ the component of v in the direction of the plasma current, and the location in space and time. Integrating over E_j and averaging over λ gives the fast ion density. Results for 100 MW of D-NBI are shown in Fig 11. Although the injection is near $v_{parallel} = v$ (along the plasma current), the equilibrium distribution has considerable density at lower $v_{parallel} / v$.

Profiles of the plasma heating power densities during the NBI phase are shown in Figs. 12. The fusion power and heating powers of two cases are compared in Table II. The total alpha heating power is 20% of the total fusion power. The total beam heating and thermalization powers are 100 MW. The global and central alpha heating powers are considerably greater than the NBI heating powers so these plasmas are near or past ignition

conditions.

The stored energies, energy confinement times, and β_{norm} values are compared in Table III. The energy confinement time is defined as the ratio of the total (thermal and fast ion) plasma energy and the total heating power. The transport coefficients of the thermal plasma are calculated from the profile gradients and the energy, momentum, and species fluxes. At radii where the profiles are not decreasing monotonically, large positive or negative values for the difusivities can result. Examples are shown in Figs. 13. The coefficients must be lower for the cases without auxiliary heating. In the flat profile case, Fig. 13-a, χ_e and χ_{ion} are about 100 times the neo-classical value χ_{NC} over much of the profile. For the peaked profile case, Fig. 13-b, the effective particle diffusivity D_e must be considerably lower than χ_{NC}. The values for χ_e and χ_{ion} are in rough agreement with the values in the ITER interim database.

The profiles of the currents are shown in Fig. 14. The beam-driven current for with 50 MW of D-NBI is approximately 0.6 MA. The bootstrap contributions are relatively small. Examples are compared in Table IV. A large Ohmic, or otherwise driven current is necessary to provide the total current of 21 MA.

5. Sawteeth Effects

It is not known whether ITER discharges will exhibit sawteeth, or how they will respond to sawteeth crashes. There is extensive empirical data on sawteeth effects in current Tokamaks. For simplicity, we assume that the densities and temperatures of the thermal species are not altered, contrary to empirical observations in Tokamaks. We use TRANSP to simulate sawtooth effects on the current and fast ion profiles.

The sawtooth period is assumed to be 50 sec. The amount of current mixing during sawteeth crashes can be varied in TRANSP. In modeling TFTR discharges, about 20-30% current mixing gives approximate agreement with measurements. Examples of the evolutions of $q_\psi(0)$ for ITER with two different assumptions are shown in Fig. 15. If the amount of current mixing will be as small, as in TFTR, many sawteeth crashes are needed to raise $q_\psi(0)$ to values near 1. The current relaxation time is very long, so the decay of $q_\psi(0)$ after each crash is not large even with periods of 50 sec. The $q_\psi = 1$ surface is calculated to be around x = 0.25 - 0.35. The q_ψ profiles are shown in Fig. 16.

Sawteeth effect the distribution of alphas in TFTR [22,23,24]. The dynamics of this effect is complicated [25], but a simple model has been incorporated into TRANSP [5]. The effect of sawtooth crashes on the fast alpha density computed by TRANSP is shown in Fig. 17. The recovery of the alpha fusion power and alpha heating profiles will depend on details of how the temperatures and the D, T, impurities, and alpha densities are redistributed,

and how the transport evolves since these determine the subsequent reheating.

6. Ripple Effects

The magnitude of the toroidal ripple field is shown in Fig. 2. The fast-ion ripple losses are estimated in TRANSP by assuming the ions are lost if their turning points are in regions with ripple exceeding an empirical factor times the Goldston-White-Boozer (GWB) [26] threshold. The model has not yet been generalized for up/down asymmetric plasmas. The threshold has been renormalized [7] by comparing losses obtained [6] with TRANSP and with the Hamiltonian guiding-center code ORBIT [24, 25]. The thresholds that give agreement for TFTR supershots are 1/2*GWB for the fast alpha particles and 4*GWB for the beam ions. The actual threshold renormalization is strongly collisionally dependent on the artificial pitch angle acceleration level used in TRANSP [7]. Similar renormalization for ITER discharges with appropriately higher statistics indicates that the threshold for alpha particles is 1/2*GWB (as in TFTR), not 1*GWB [27].

The prediction for the steady state phases of ITER discharges is that 3% of the alpha energy and 5% of the fast alpha particles are ripple lost. A comparable fraction of the beam ion energy is predicted to be ripple lost. If the fast alphas are redistributed by sawtooth crashes, the ripple loss is expected to increase. With the flat redistribution shown in Fig. 17, the ripple loss is predicted to increase by a factor of three-four [27]. The duration of this increased loss depends on the dynamics of recovery of the alpha profile to the pre-crash state. This depends on unknown details of the plasma recovery.

7. Alpha Ash

The transport of the thermal ash was varied to find transport coefficients that generate equilibrium ash profiles consistent with 1.5 GW of fusion power. The diffusivity and radial pinch velocity profiles for the ash density are defined from their density and net flux profiles:

$$\gamma_{He} = - D_{He}\, \mathrm{grad}(n_{He}) + V_{He}\, n_{He} \qquad (1)$$

The evolution of the volume integral to the separatrix of the ash density is given by

$$F(dN_{He},dt) = S_{th} + \Gamma_{in} - \Gamma_{out} = S_{th} - \Gamma_{pump} \qquad (2\text{-a})$$

$$\Gamma_{in} = R_{rec}\, \Gamma_{out} \qquad (2\text{-b})$$

$$\Gamma_{pump} = (1 - R_{rec})\Gamma_{out} \qquad (2\text{-c})$$

S_{th} is the volume integral of the alpha thermalization rate. TRANSP calculates the alpha thermalization rate profiles to be close to the DT fusion rate, as shown in Fig. 8. The thermal He fluxes in and out the separatrix are Γ_{in} and Γ_{out}. The recycling coefficient R_{rec} and the pumping rate Γ_{pump} are the average values on the separatrix surface. In steady state, the averages at the separatrix are the averages at the pump entrances.

The global He confinement times at the separatrix are defined as:

$$\tau_{He} = N_{He} / \Gamma_{out} \qquad (3\text{-a})$$

$$\tau^*_{He} = N_{He} / \Gamma_{pump} = \tau_{He} / (1 - R_{rec}) \qquad (3\text{-b})$$

Results from experiments with TFTR supershots indicate that n_{He} is relatively flat compared with n_e [28]. The transport coefficients consistent with these measurements have $D_{He}(x) \sim D_e(x) \sim \chi_{eff}(x)$ (the effective energy transport coefficient). The radial pinch $V_{He}(x)$ has relatively small values for $x < 0.5$, and anomalously large negative values for $x > 0.6$. The recycling coefficient consistent with these measurements is $R_{rec} \cong 0.85$, and the ratio $\tau^*_{He} / \tau_E \cong 6$.

It is not clear how the existing Tokamak results scale to ITER discharges. For instance, $D_e << \chi_{eff}$ might be expected in ITER (see Fig. 13-b) , but $D_{He} << \chi_{eff}$ would imply large accumulations of He ash. Because of these uncertainties, we studied a range of He transport coefficients. It is inefficient to use TRANSP to scan in the ratio D_{He} / χ_{eff} since χ_{eff} changes as the n_{He} / n_e ratio and the alpha heating change. A simpler assumption is used here: scans with constant D_{He} and V_{He} are studied. For most of the runs the pinch is assumed to be negligible.

Another uncertainty for ITER is the He recycling coefficient. Estimates for this range up to $\cong 0.99$. High values lead to pessimistic requirements for the He transport. We first discuss results for the optimistic assumption $R_{rec} = 0.5$, and then indicate how the requirements change as R_{rec} increases.

Each TRANSP run used a fixed D_{He} and V_{He} and initial conditions chosen to speed the convergence to steady state n_{He} profiles. One measure of equilibrium is $S_{th} / \Gamma_{pump} = 1$. The runs reported here converged sufficiently so that $S_{th} / \Gamma_{pump} = 1$ to within 8%. As D_{He} increases, N_{He}, τ_{He}, and τ^*_{He} decrease, whereas Γ_{pump} and P_{DT} increase. These dependencies are shown in Fig. 18. For the flat profile case shown in Fig. 13-a, D_{He} needs to be at least 2 m^2/s for 1.5 GW, which is comparable to χ_{eff} near $x = 0.5$. For the peaked case in Fig. 13-b, D_{He} needs to be at least 0.4 m^2/s, which is considerable lower than χ_{eff}

with NBI.

Ash parameters are summarized in Table V. As D_{He} increases, τ_E / τ^*_{He} increases. The corresponding increase in P_{DT} is shown in Fig. 19. This ratio needs to be smaller than about 16 to achieve P_{DT} = 1.5 GW with the plasma and recycling we assume.

The runs discussed above have R_{rec} = 0.5 and negligible V_{He}. As R_{rec} increases towards 1, the values of D_{He} needed to achieve 1.5 GW increase. The ratio minimum τ_E / τ^*_{He} remains around 15. For R_{rec} = 0.95, the required D_{He} if the pinch is negligible increases from 2 m^2/s to 15 m^2/s for the flat profile case and from 0.4 m^2/s to 4 m^2/s for the peaked profile case. As $-V_{He}$ increases, larger values of D_{He} are needed to keep n_{He} low enough to achieve 1.5 GW. Profiles of n_{He} generated by several combinations of D_{He} and V_{He} that are consistent with R_{rec} = 0.97 and 1.5 GW are shown in Fig. 20.

8. Summary

The TRANSP plasma analysis code is used to model the steady state phases (including periodic sawteeth) of two discharges from the ITER database. TRANSP provides comprehensive, self-consistent models for the particle, energy, and momentum balance, and computes thermal transport coefficients and alpha parameters. Several models for the transport of thermal ion species are available. The model for the relative mixing of D and T that is consistent with TFTR measurements gives pessimistic results for ITER. Results assuming equal D and T transport are assumed here. Effects of 50 MW of D-NBI at 1 MeV are studied. The heating occurs near the mid radius, and the average energy of the beam ions is approximately one-half the injection energy. The beam-driven currents are ~ 0.6 MA for this voltages. The beam ions contribute significantly to the ion and electron heating in the region around x = 0.8.

The q_ψ = 1 radius is calculated to occur near the x = 0.3 - 0.5 flux surface. The amount of current mixing and the sawtooth period significantly effect the $q_\psi(0)$ value. Sawteeth crashes are modeled to significantly redistribute the fast ion density profiles.

Toroidal field ripple is estimated to cause losses of ~ 3% of the alpha energy and ~ 5% of the fast alpha particles. If the fast alphas are redistributed by sawtooth crashes, the ripple losses are predicted to increase by about a factor of about three transiently.

The alpha ash is modeled assuming constant transport coefficients with a range of values. The ratio of the confinement times, τ^*_{He} / τ_E needed to achieve steady state fusion powers of 1.5 GW with the assumed density and temperature profiles is ≤ 15. The required ash diffusivity D_{He} depends strongly on the pinch and the average recycling coefficient. If the pinch is negligible and if $R_{rec} \leq 0.5$, then values of D_{He} comparable to those measured in current Tokamak experiments is sufficient. If R_{rec} is much larger, then higher values are

needed. Accurate modeling of R_{rec} is needed.

Acknowledgments

This work is supported by the U. S. Department of Energy for support under the Contract No. DE-AC02-76CH0-3073. We wish to thank D. Boucher, S. Kaye, M. Rosenbluth, R. White, and S. Zweben for discussions and encouragement.

Table I - Alpha Parameters

Parameter	Peaked n_e (01002D011)	Flat n_e (01001D29)
$\beta_\alpha(0)$	0.015	0.006
$<\beta_\alpha>$	0.0015	0.002
$-R*grad(\beta_\alpha)$	0.06	0.04
$n_\alpha(0) / n_e(0)$	0.005	0.003
v_α(birth) / $v_{Alfvén}$	1.9	1.7

Table II- Fusion and Heating Powers with 50 MW of 1 MeV D-NBI

	Peaked n_e (01002D11)		Flat n_e (01001D29)	
	Center (MW/m^3)	Total (MW)	Center (MW/m^3)	Total (MW)
P_{DT}	3.6	1550	1.92	1400
$P_{\alpha\text{-}e}$	0.73	215	0.50	195
$P_{\alpha\text{-}I}$	0.44	78	0.20	75
$P_{bm\text{-}e}$	0.00	32	0.00	60
$P_{bm\text{-}I}$	0.00	16	0.00	40
$P_{bm\text{-}th}$	0.01	2	0.01	2

Table III - Plasma Conditions with 50 MW of 1 MeV D-NBI

Parameter	Peaked n_e (01002D11)	Flat n_e (01001D29)
W_{tot} (GJ)	1.20	1.24
W_{el} (GJ)	0.67	0.67
W_{ion} (GJ)	0.47	0.48
W_{α}(GJ)	0.054	0.060
W_{beam} (GJ)	0.011	0.030
τE (sec)	3.41	3.35
β_{norm}	2.33	2.40

Table IV - Beam-Driven and Bootstrap Currents with 50 MW D-NBI

Current	Peaked n_e (01002D11)	Flat n_e (01001D29)
I_{beam}	1.2	3.3
I_{boot}	5.0	2.8
I_{OH}	14.8	15.0
Itotal	21.0	21.0

Table V - Thermal He Parameters for P_{DT} = 1.5 GW if R_{rec} = 0.5

Parameter	Peaked n_e (01002D11)	Flat n_e (01001D29)
D_{He} (m2 /s)	4	15
$n_{He}(0) / n_e(0)$	0.13	0.16
$n_{He}(1) / n_e(1)$	0.32	0.18
N_{He} (1022)	4.08	4.21\
T_{pump} (1020 / sec)	5.3	4.5
t_{He}(sec)	3.9	5.5
t^*_{He} (sec)	77	110

References

[1] P. H. Rebut, V. Chuyanov, M. Huguet, *et al.*, IAEA-CN-60/E-1-I-1, Fifteenth International Conference on Plasma Physics and Controlled Nuclear Fusion Research, Seville, Spain, 1994.

[2] Available on internet at http://picard.iterus.org.

[3] R. V. Budny, M. G. Bell, R.E. Bell, et *al.,* "TRANSP Analysis of High Fusion Power TFTR DT Supershots", PPPL-3039.

[4] D.C.McCune, R.J. Goldston, R.T. McCann, R.M. Wieland, *et al.,* Bulletin American Physical Society, **39** (1994) 1680.

[5] R. V. Budny, M. G. Bell, R.E. Bell, *et al.,* PPPL-3112, to be published in Nucl. Fusion.

[6] M. H. Redi, M.C. Zarnstorff, *et al.*, Nucl. Fusion **35** (1995) 1191.

[7] M. H. Redi, R.V. Budny, *et al.*, accepted for publication in Nucl. Fusion.

[8] M. H. Redi, R.V. Budny, *et al.*, EPS, Bournemouth (1995).

[9] R. B. White and M. Chance, Physics of Fluids, (1984) and R. B. White, Physics of Fluids (1990).

[10] R.C. Grimm, *et al.,* J. Comput. Phys. **49** (1983) 94.

[11] C.Z. Cheng, *et al.,* Fourteenth International Conference on Plasma Physics and Controlled Nuclear Fusion Research, Wurzburg, 1992.

[12] R. V. Budny, M. G. Bell, H. Biglari, *et al.*, Nucl. Fusion **32** (1992) 429.

[13] B. Balet, P. M. Stubberfield, D. Borba, *et al.,* Nuclear Fusion,**33** (1993) 1345.

[14] B. LeBlanc, *et al.*, Nucl. Fusion, **33** (1993) 1645.

[15] J. Ongena, H. Conrads, M. Gaigneaux, *et al.*, Nucl. Fusion **33** (1993) 283.

[16] G.T. Hoang, C. Gil, E. Joffrin, *et al.*, Nucl. Fusion **34** (1994) 75.

[17] M. Greenwald,R.L. Boivin, P. Bonoli, *et al.*, Physics of Plasmas **2 (1995) 2308**.

[18] R. V. Budny, Sherwood Meeting, Santa Fe April, 1990.

[19] R. V. Budny, L. Grisham, D.L. Jassby, *et al.*, proceedings of the 19th EPS conference, Innsbruck (1992) I-43.

[20] R. V. Budny, Nucl. Fusion **34** (1994) 1247.

[21] R. V. Budny, *et al.,* "Tritium Transport and Recycling in TFTR Discharges", in preparation.

[22] R. Fisher, J. M. McChesney, P. B. Parks, *et al.*, Phys. Rev. Letter **75** (1995) 846.

[23] M. Petrov, R.V. Budny, H.H. Duong, *et al.*, "Studies of Energetic Confined ALphas

Using the Pellet Charge Exchange Diagnostic on TFTR",submitted in Nucl. Fusion.

[24] S. Medley, R. V. Budny, D. K. Mansfield,*et al.*, EPS Bournemouth (1995).

[25] R. White and Y. Zhao, in preparation.

[26] R. J. Goldston, R. B. White, and A. H. Boozer, Phys. Rev. Lett. **47** (1981) 647.

[27] M. H. Redi,*et al.*, "Ripple Loss Simulations of Alpha Particles from ITER", in preparation.

[28] E.J. Synakowski, R.E. Bell, R.V. Budny,*et al.*, Phys. Rev. Letters **75** (1995) 3689.

Figure Captions

Fig. 1 Assumed boundary flux surface (for instance, for the 98% flux surface) and the interior flux surfaces calculated solving the Grad-Shafranov Equation for the MHD equilibrium. The flux surfaces for both the flat and peaked categories of discharges are very similar.

Fig. 2 Assumed toroidal ripple field and the location of the plasma boundary.

Fig. 3 Comparison of the assumed electron density profiles for the flat and peaked cases.

Fig. 4 Assumed profiles for a) Z_{eff} and b) P_{rad} for the flat and peaked density cases.

Fig. 5 Comparison of the assumed temperature profiles for the a) flat and b) peaked cases.

Fig. 6 Density profiles for the a) flat and b) peaked density cases with P_{DT} = 1.5 GW and 100 MW of D-NBI at 1 MeV. The assumed electron density and the calculated thermal D, T, He, and impurity, and fast D and He densities are shown.

Fig. 7 Beam deposition rate profiles for the peaked density cases with 100 MW at 1 MeV for a) flat and b) peaked discharges. The dominant rates are ionizations of the thermal D and T, electrons, and impurities. Charge-exchange rates are lower.

Fig. 8 Fusion power profiles for the peaked and flat density cases with P_{DT} = 1.5 GW.

Fig. 9 Slowing down profiles for the birth alphas and beam ions.

Fig. 10 Average energy profiles for the fusion alpha particles and beam ions.

Fig. 11 Distribution in energy and λ = cos(pitch angle) at x = 0.0 of the beam ions from 100 MW of 1 MeV D-NBI.

Fig. 12 Heating power density profiles for the peaked density cases with 100 MW of 1 MeV D-NBI achieving P_{DT} = 1.5 GW.

Fig. 13 Transport coefficients for the electrons and thermal ions calculated from the stored energy and heating profiles for a) the flat density, and b) the peaked density cases with P_{DT} = 1.5 GW and 100 MW of D-NBI at 1 MeV.

Fig. 14 Current density profiles for a peaked density case with 100 MW of 1 MeV D-NBI a) the flat density, and b) the peaked density cases.

Fig. 15 Evolution of $q_\psi(0)$ with alternative assumptions about the fraction of current mixing during sawteeth crashes.

Fig. 16 Computed q_ψ profiles with alternative assumptions about the fraction of current mixing during sawteeth crashes.

Fig. 17 Computed change in the fast alpha density during sawteeth crashes for a) the flat density profile case, and b) the peaked density profile case.

Fig. 18 Dependencies of a) He pumping, b) the ratio τ_{He} / τ_E, c) the ratio τ_E / τ^*_{He}, and d) the fusion power on the thermal He particle diffusivity if R_{rec} = 0.95.

Fig. 19 Dependence of the fusion power on the ratios of a) τ_E / τ^*_{He}, and b) τ^*_{He} / τ_E if R_{rec} = 0.5.

Fig. 20 Examples of D_{He} and V_{He} that produce steady state n_{He} profiles for the peaked n_e case with P_{DT} = 1.5 GW and R_{rec} = 0.97. When $-V_{He}$ is large, both the D_{He} and V_{He} terms in Eq. (1) are large with opposite signs.

ITER Flux Surfaces

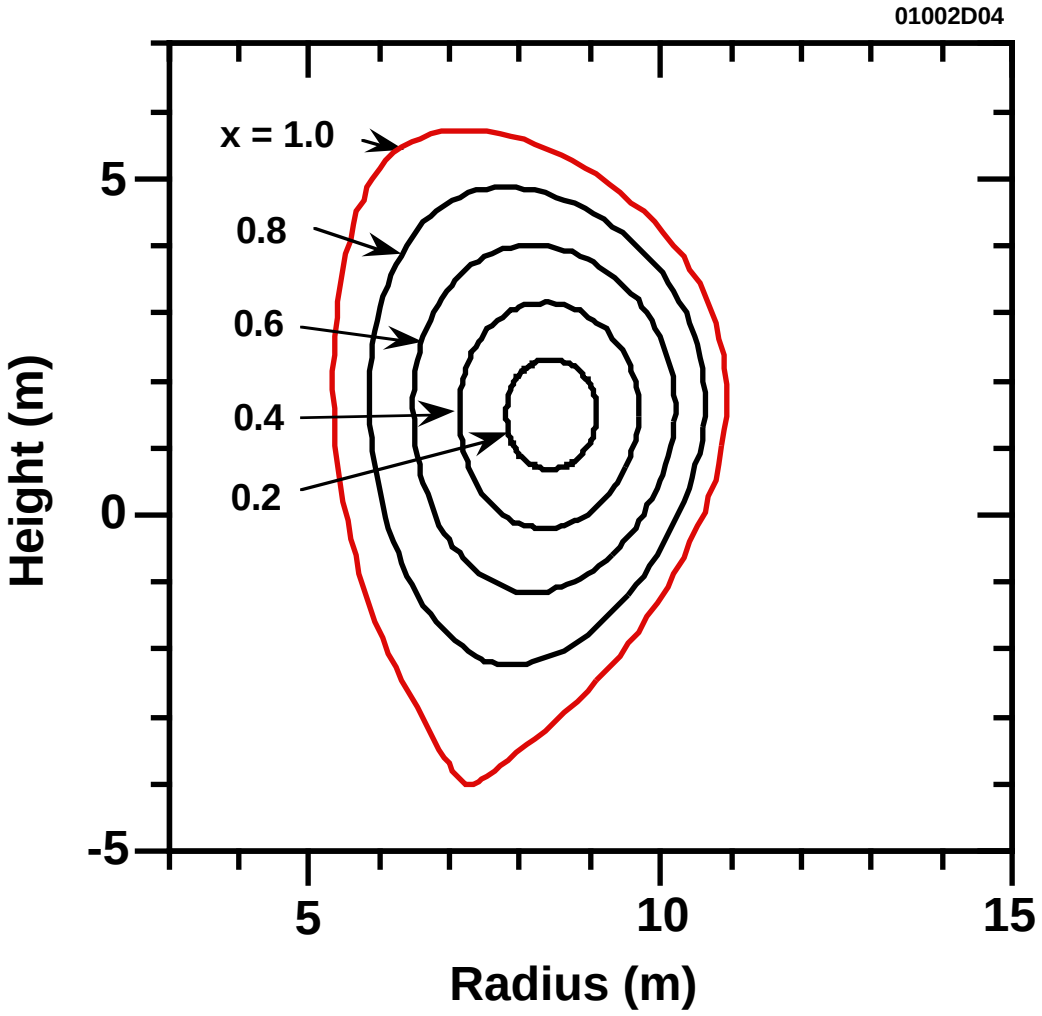

Fig. 1

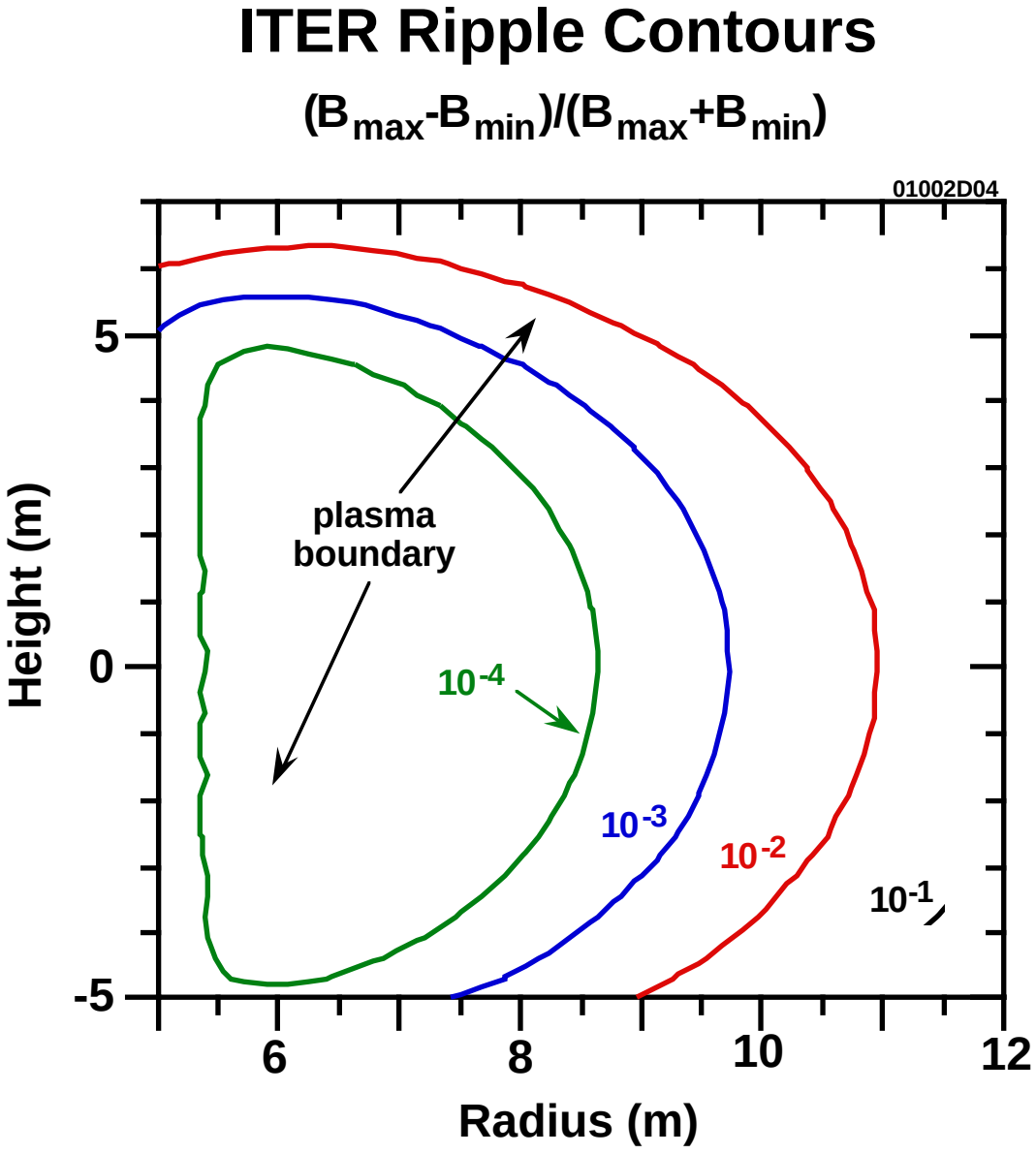
ITER Ripple Contours
(Bmax-Bmin)/(Bmax+Bmin)
01002D04
plasma
boundary
10-4
10-3
10-2
10-1
Height (m)
5
0
-5
6
8
10
12
Radius (m)

Fig. 2

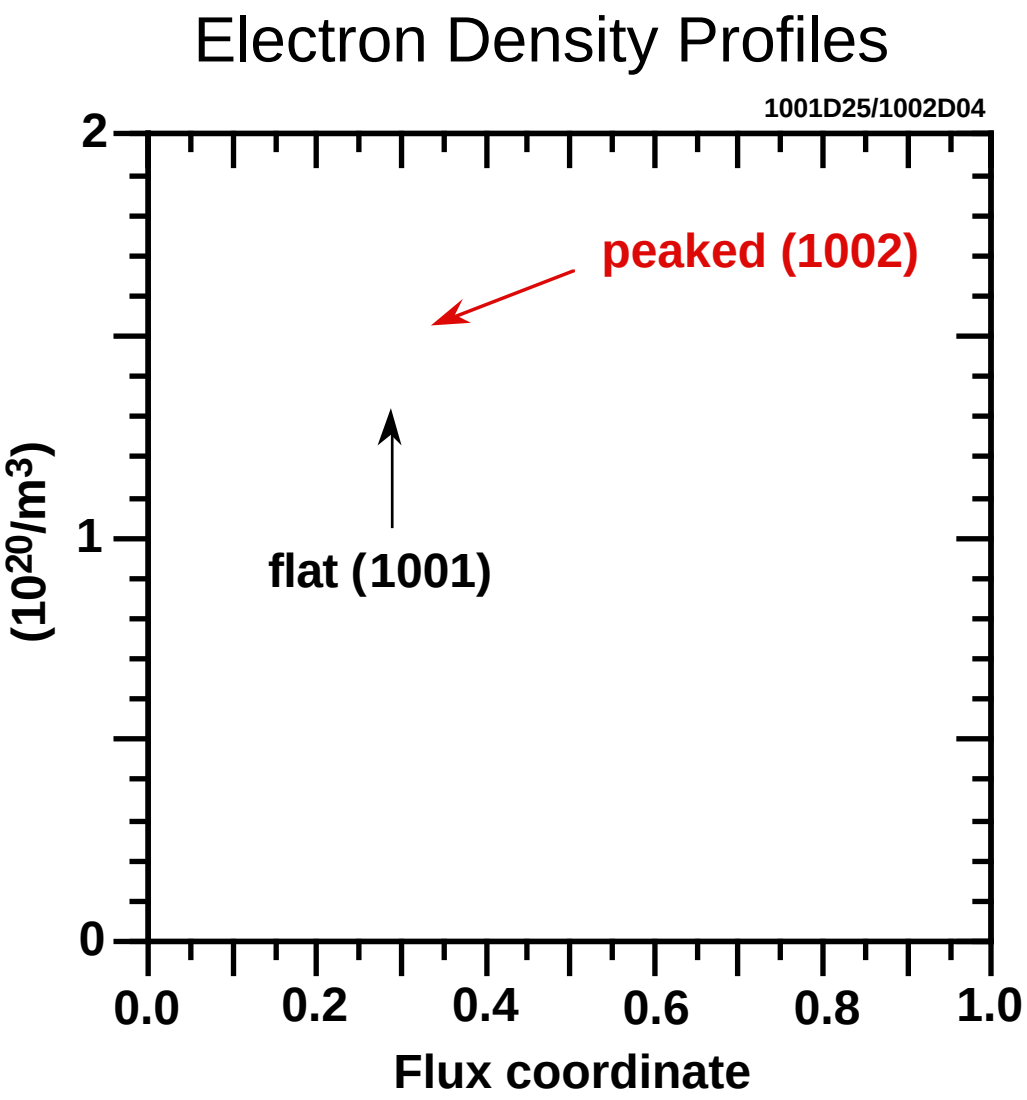
Electron Density Profiles
1001D25/1002D04
peaked (1002)
flat (1001)
(10^20/m^3)
2
1
0
0.0
0.2
0.4
0.6
0.8
1.0
Flux coordinate

Fig. 3

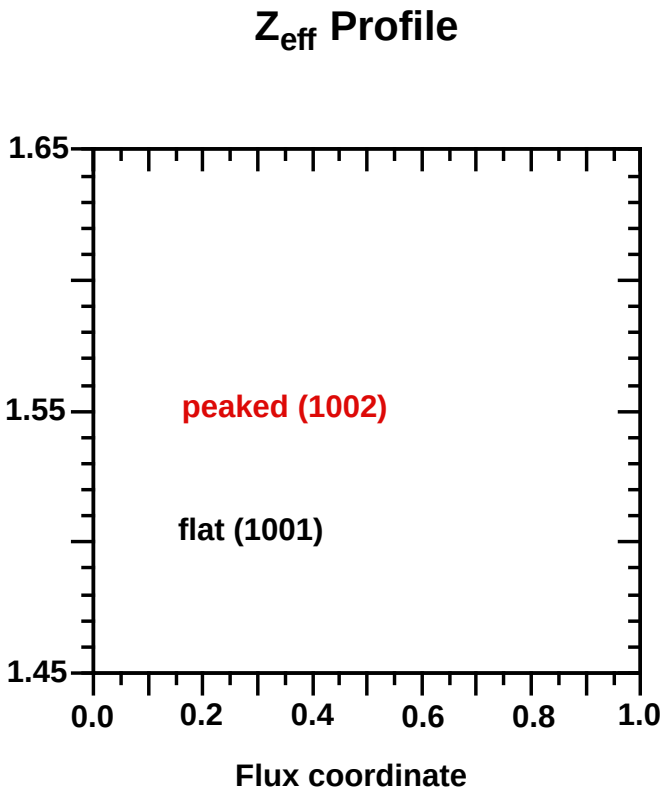
Z_{eff} Profile
1.65
1.55
1.45
peaked (1002)
flat (1001)
0.0
0.2
0.4
0.6
0.8
1.0
Flux coordinate

Fig. 4-a

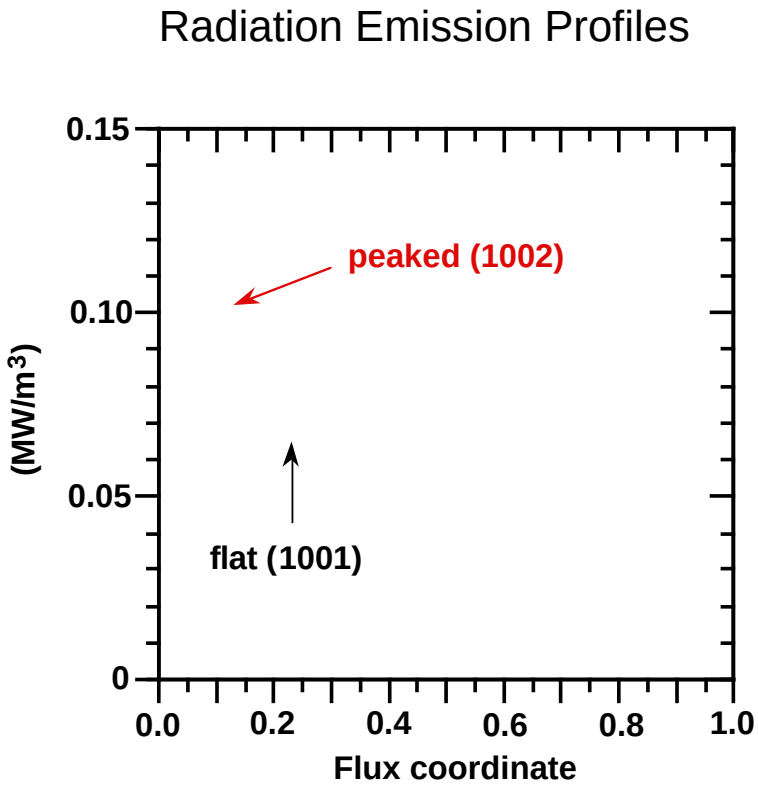
Radiation Emission Profiles
0.15
0.10
0.05
0
(MW/m^3)
peaked (1002)
flat (1001)
0.0
0.2
0.4
0.6
0.8
1.0
Flux coordinate

Fig. 4-b

ITER Temperature Profiles

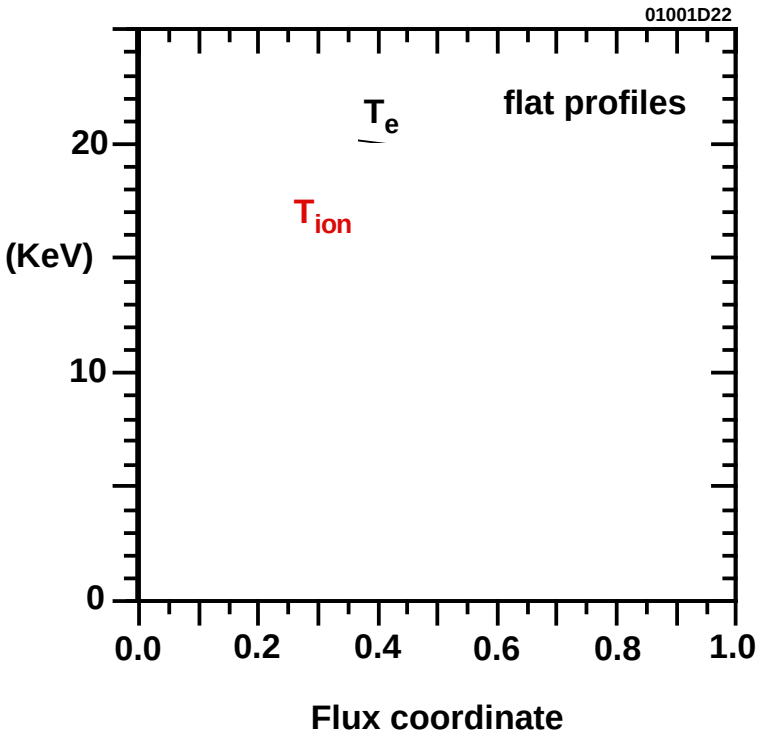

Fig. 5-a

Temperature Profiles

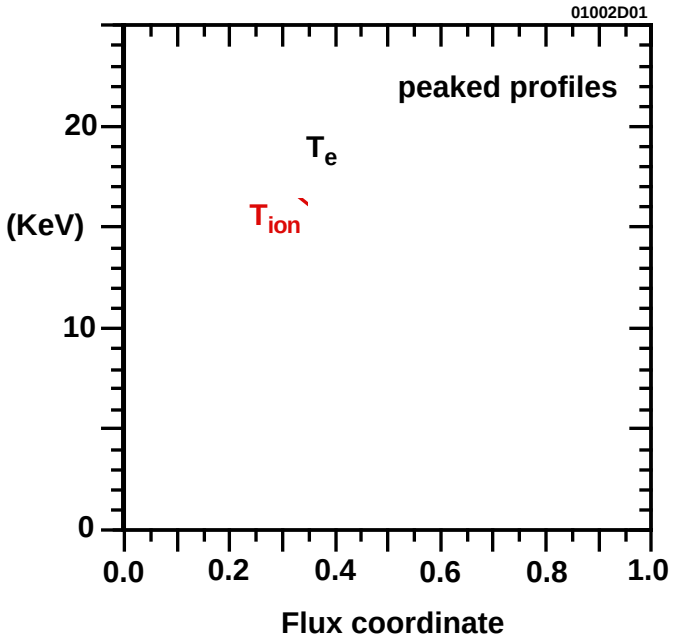

Fig. 5-b

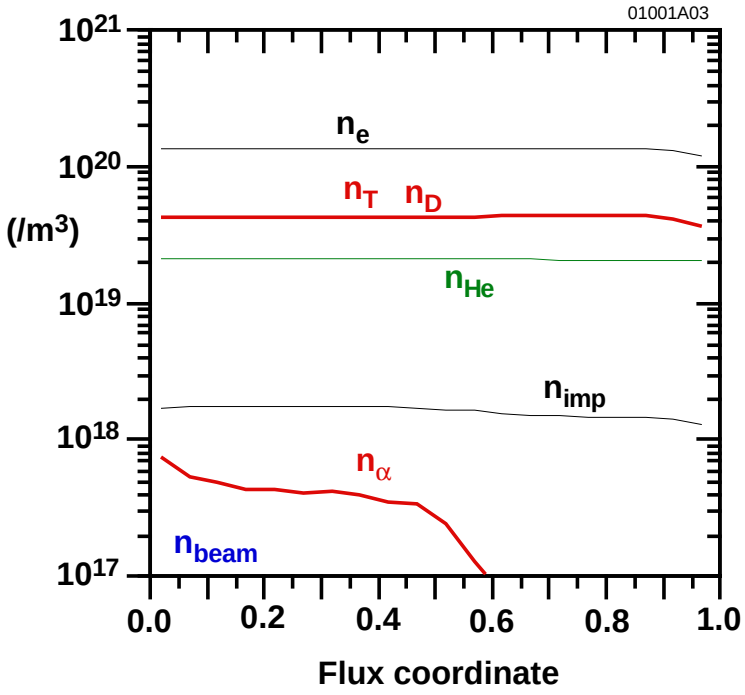
ITER Density profiles
Case of flat profiles and 100 MW D-NBI
01001A03
10^{21}
10^{20}
(/m^3)
10^{19}
10^{18}
10^{17}
n_e
n_T n_D
n_{He}
n_{imp}
n_α
n_{beam}
0.0
0.2
0.4
0.6
0.8
1.0
Flux coordinate

Fig. 6-a

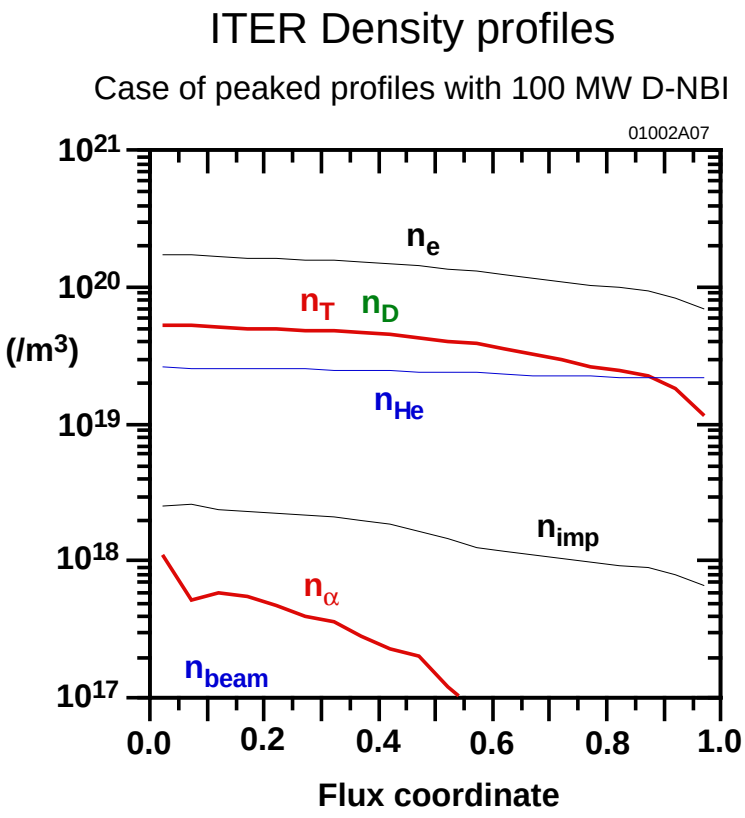
ITER Density profiles
Case of peaked profiles with 100 MW D-NBI
01002A07
10^{21}
10^{20}
(/m^3)
10^{19}
10^{18}
10^{17}
n_e
n_T n_D
n_{He}
n_{imp}
n_α
n_{beam}
0.0
0.2
0.4
0.6
0.8
1.0
Flux coordinate

Fig. 6-b

NBI Deposition Rate Profile

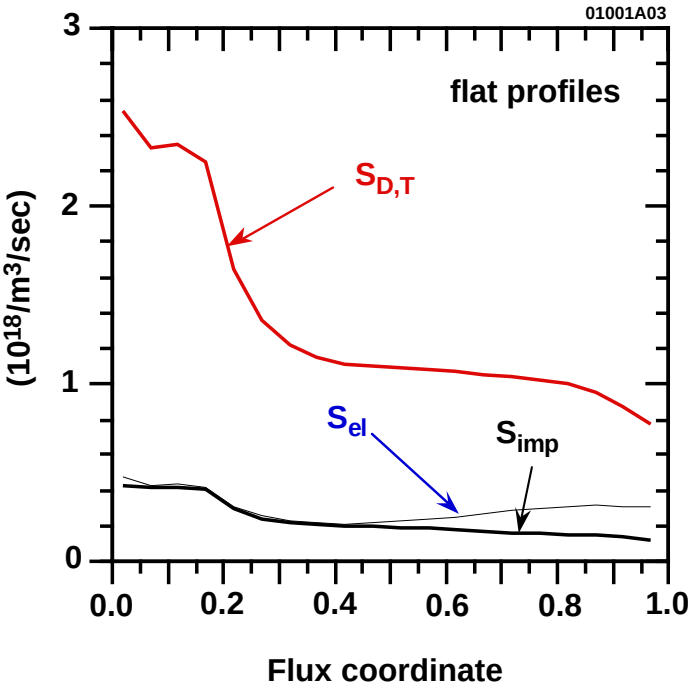

Fig. 7-a

NBI Deposition Rate Profile

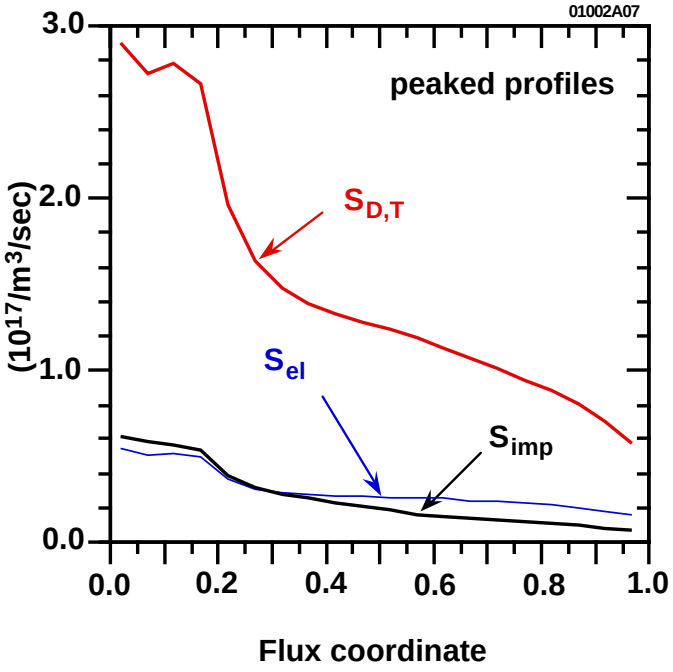

Fig. 7-b

Fusion Power Profile

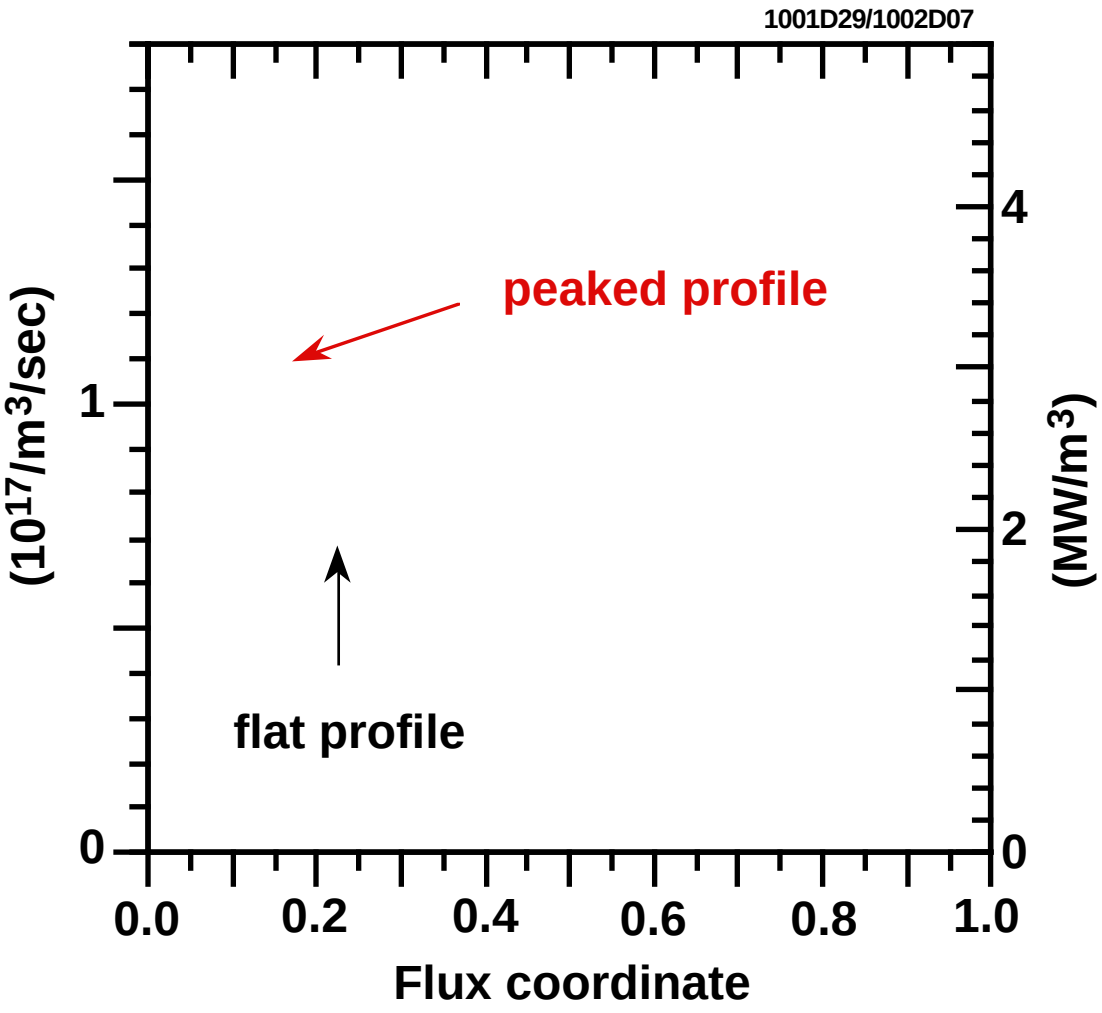

Fig. 8

Slowing Down Profiles

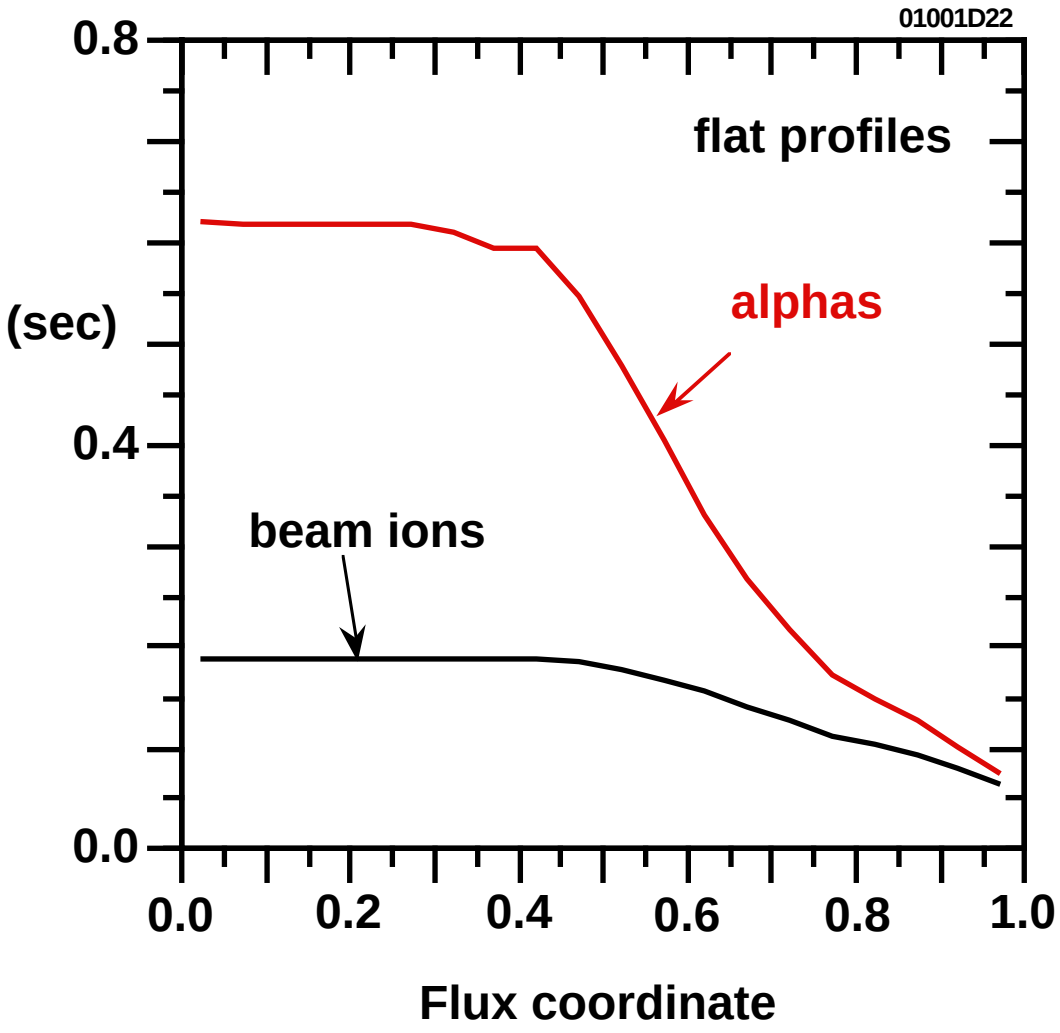

Fig. 9

Average Energy Profiles

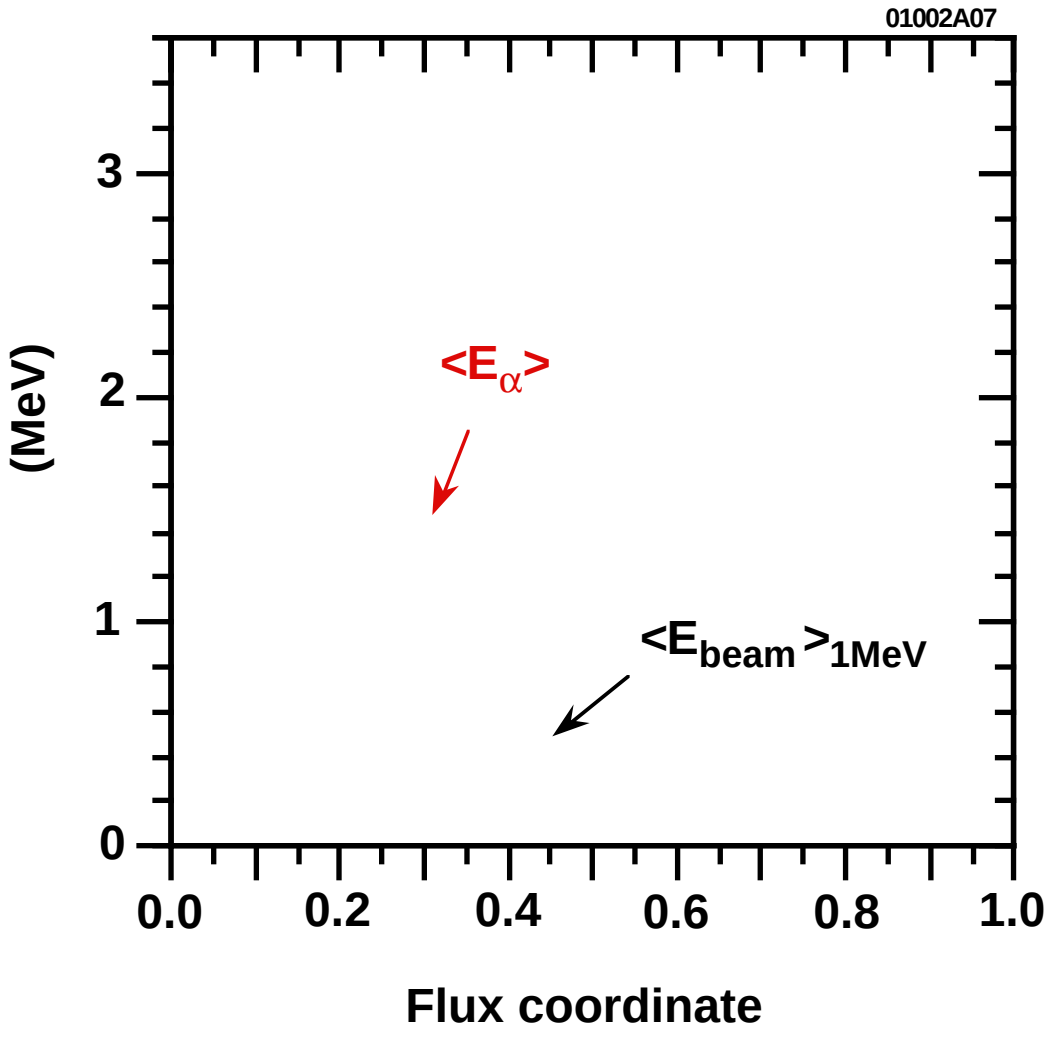

Fig. 10

D-NBI distribution at x = 0.0

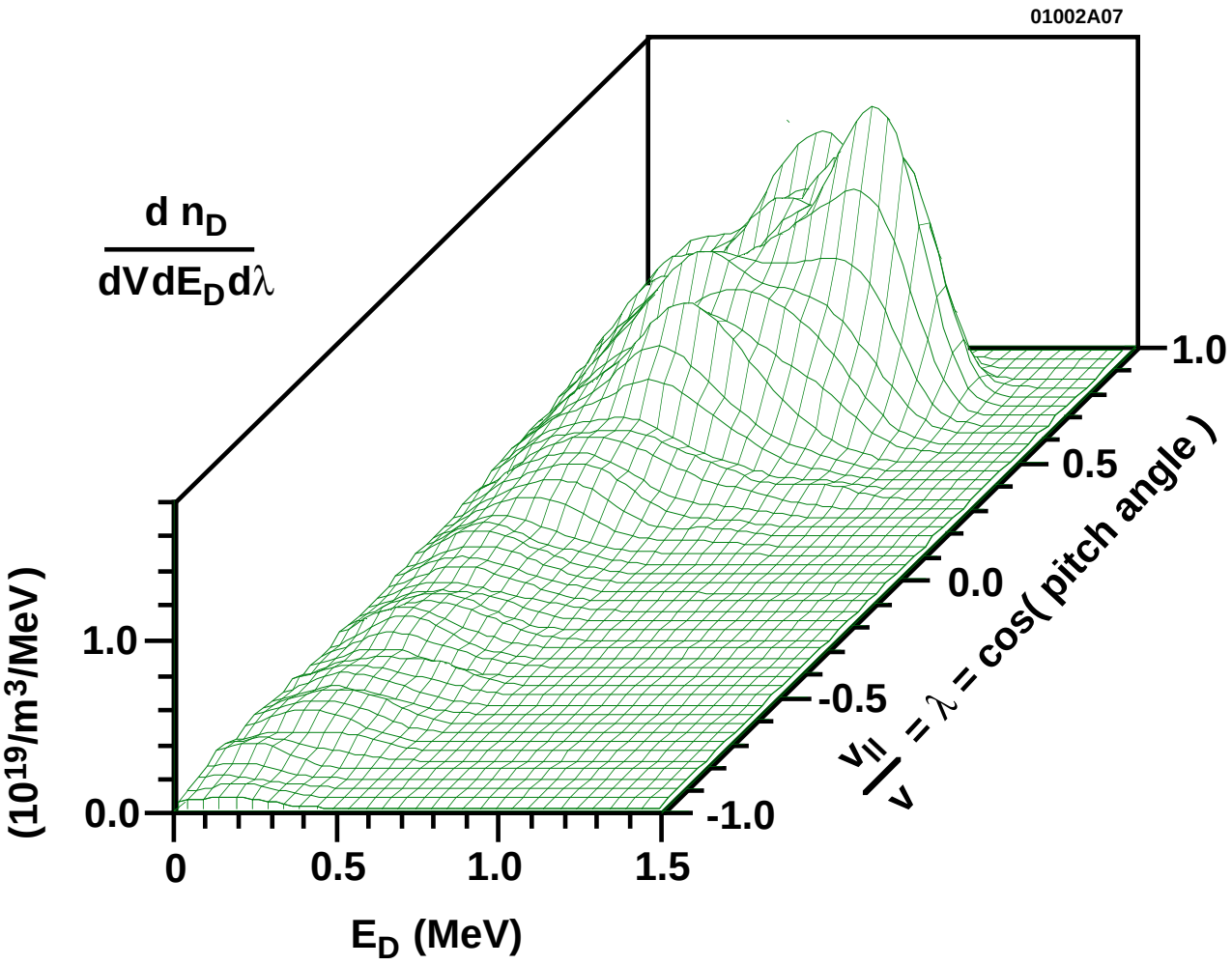

Fig. 11

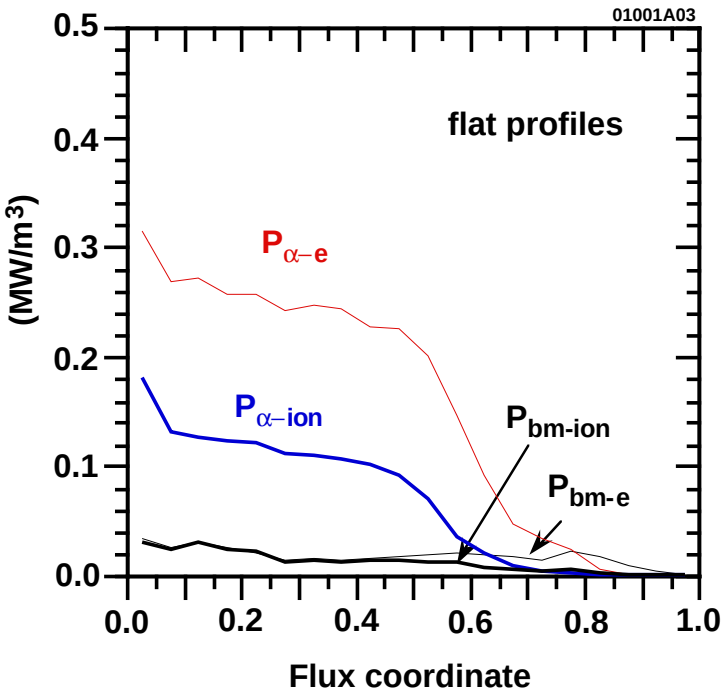

Fig. 12-a

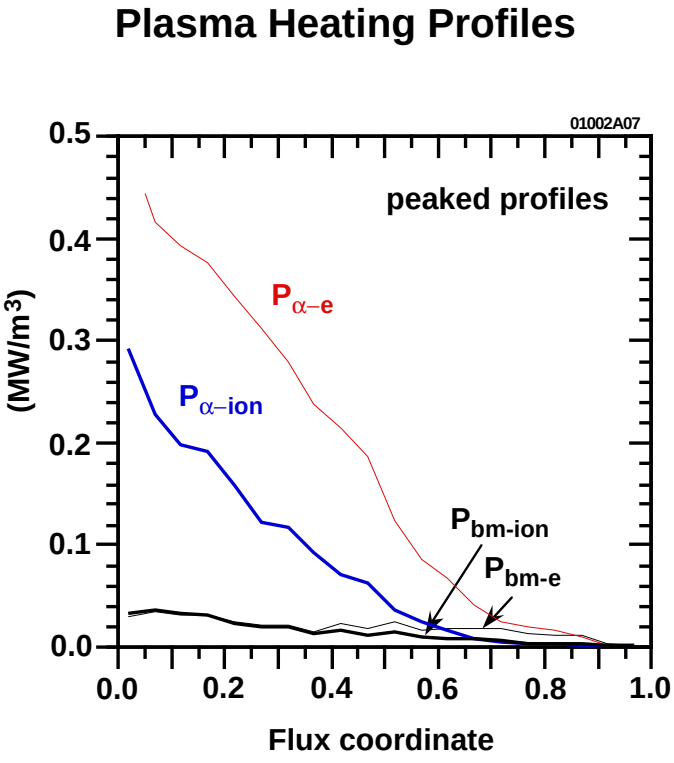

Fig. 12-b

Transport Coefficient Profiles

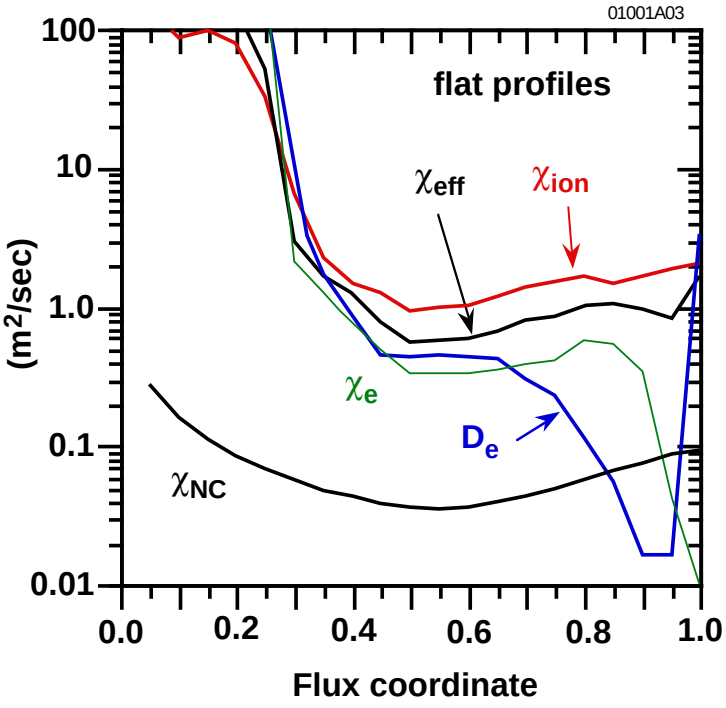

Fig. 13-a

Transport Coefficient Profiles

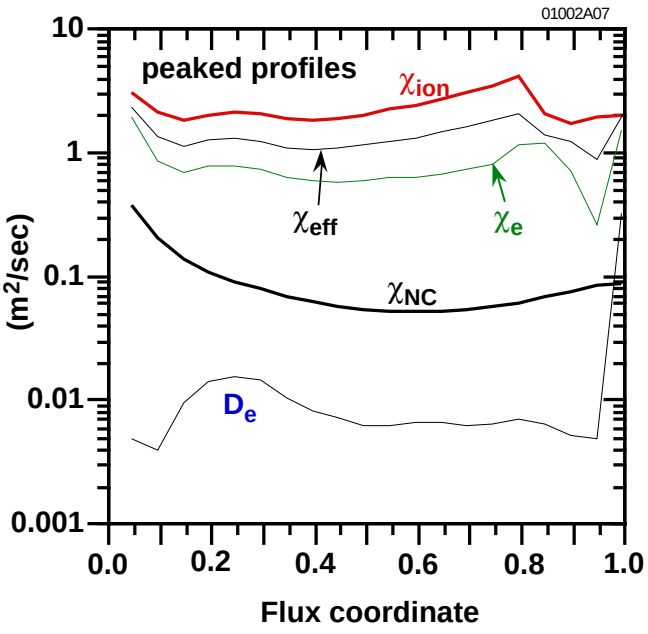

Fig. 13-b

ITER Current Profiles

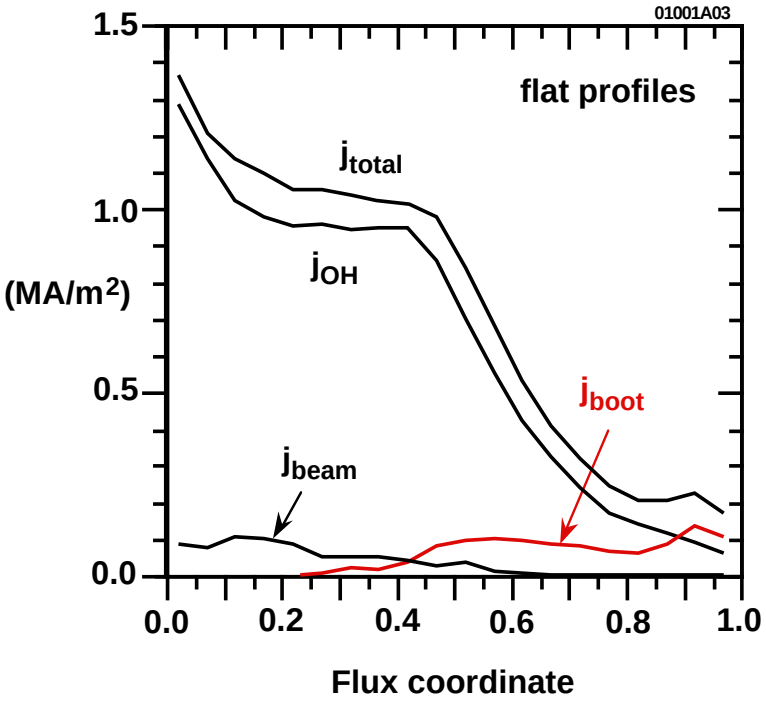

Fig. 14-a

Current Profiles

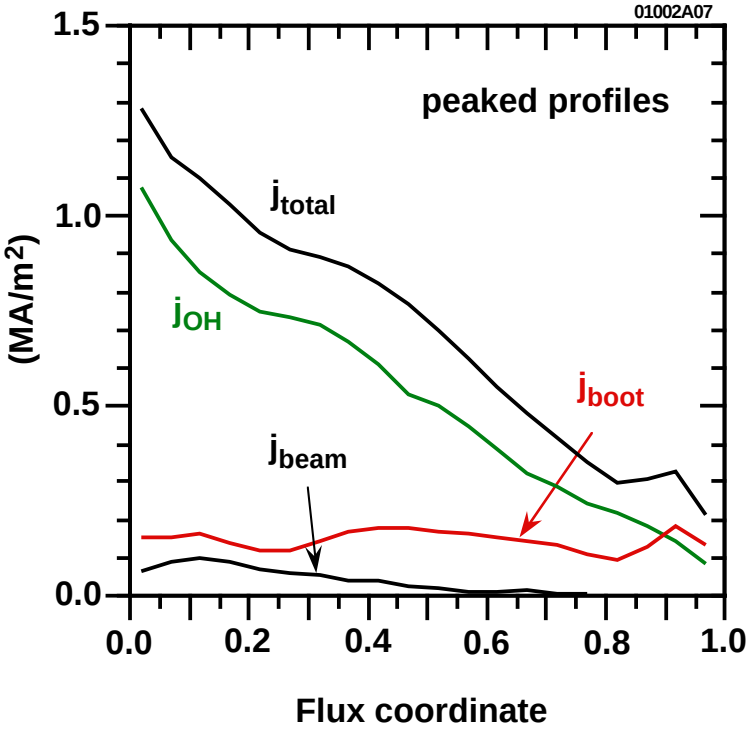

Fig. 14-b

$q_\psi(t)$ evolution

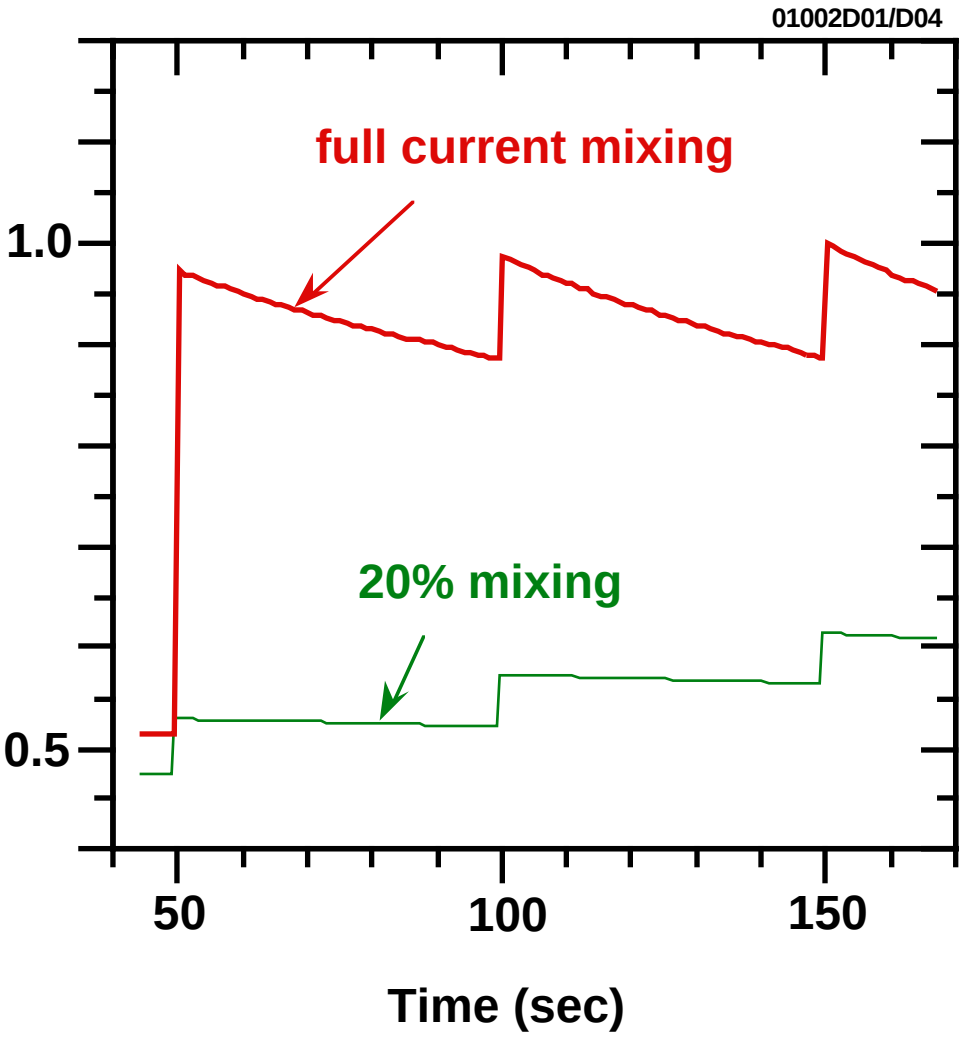

Fig. 15

q_ψ Profile

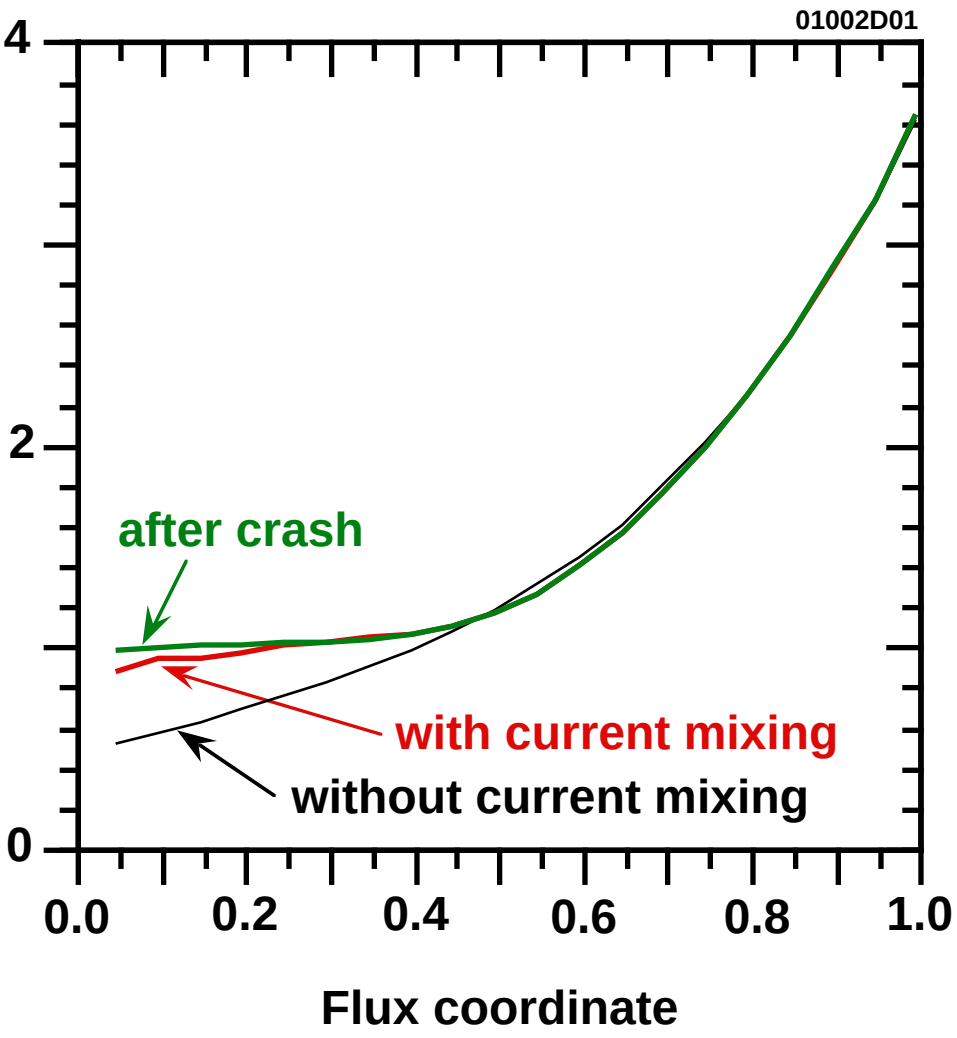

Fig. 16

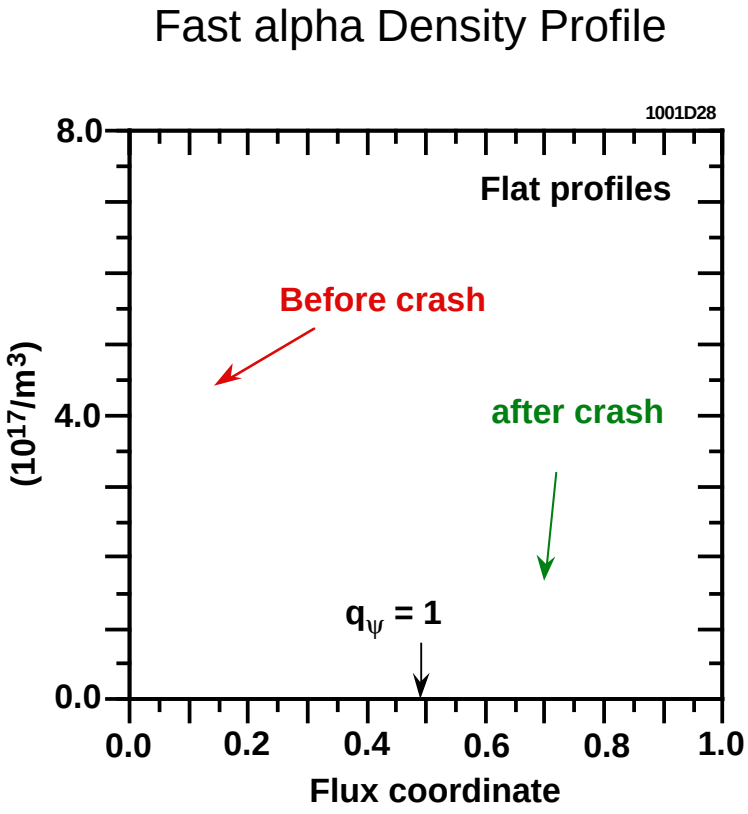

Fig. 17-a

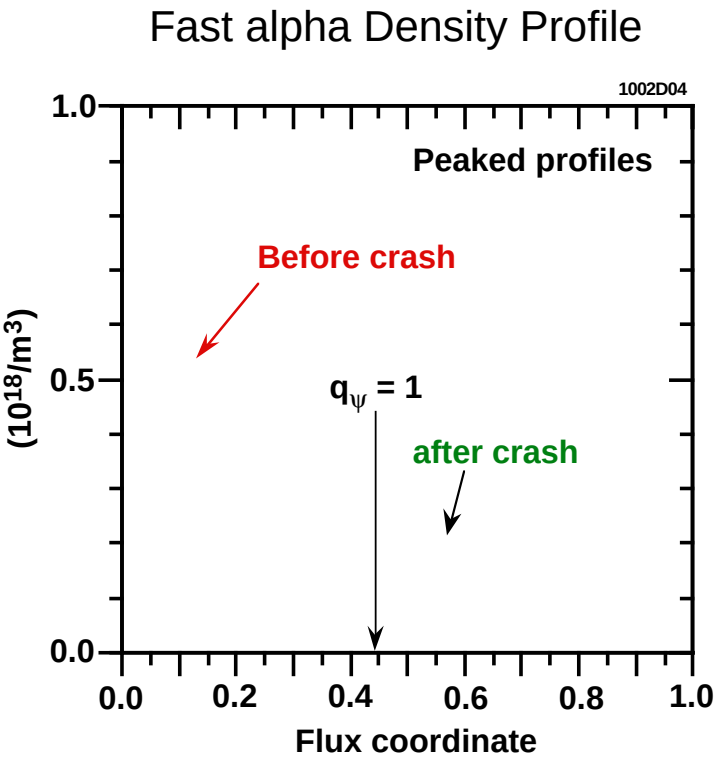

Fig. 17-b

Separatrix pumping speed

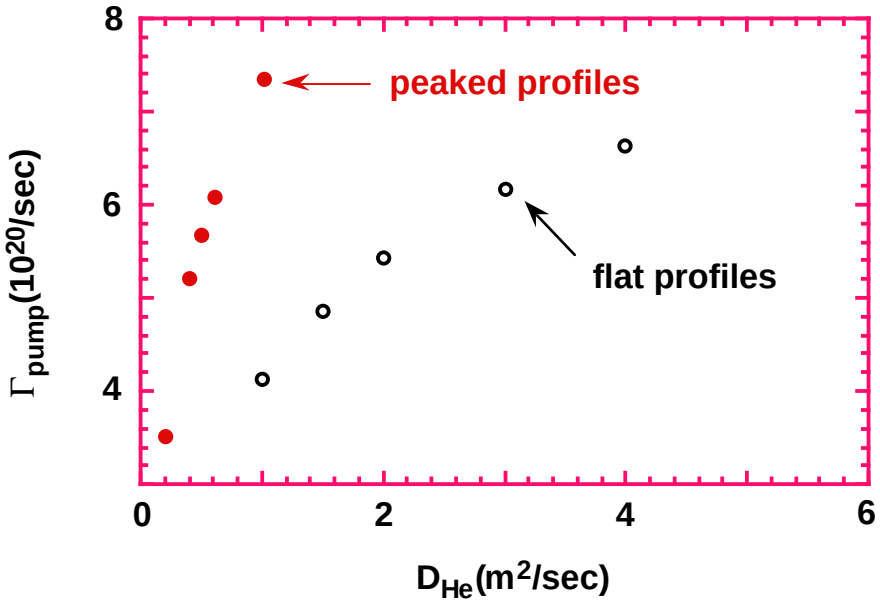

Fig. 18-a

Confinement time ratio

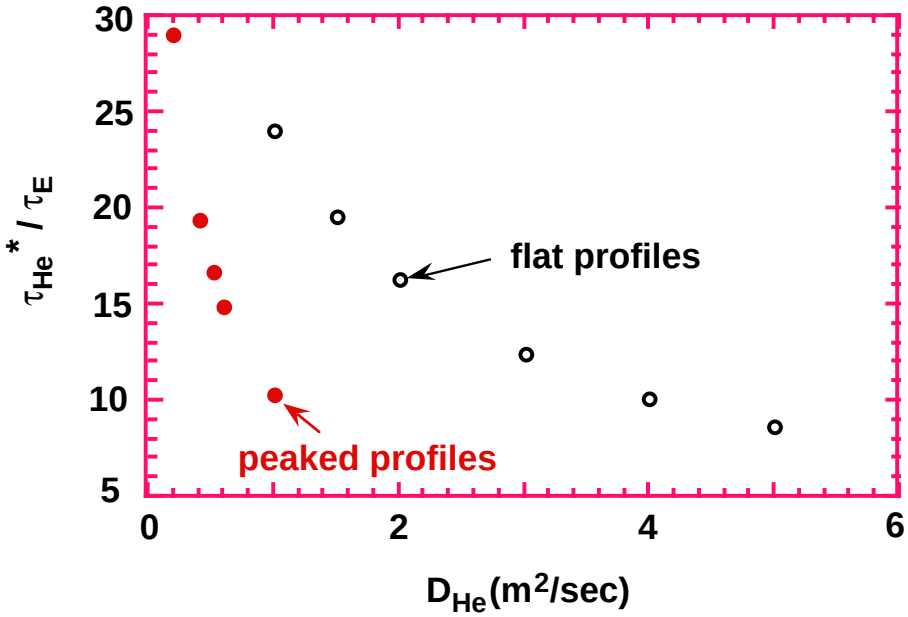

Fig. 18-b

Confinement time ratio

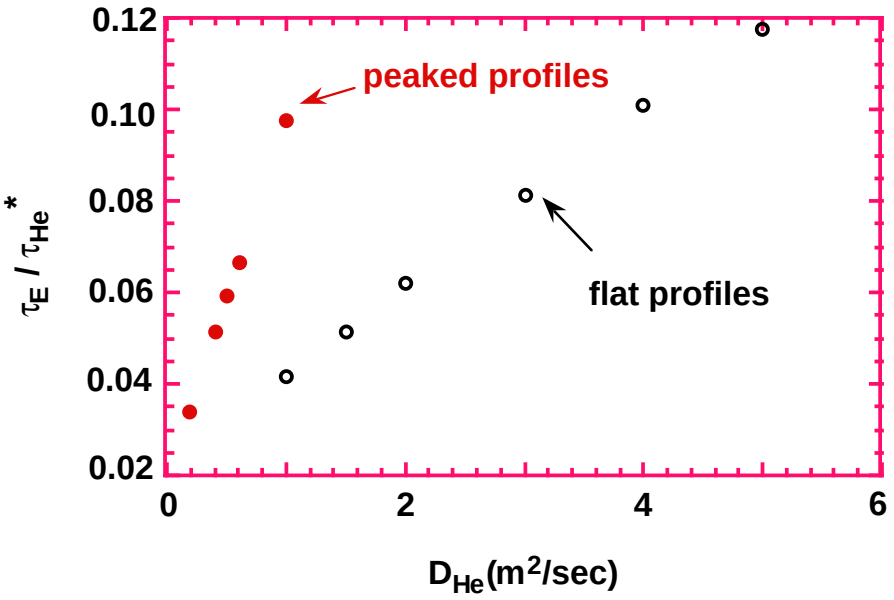

Fig. 18-c

Fusion Power

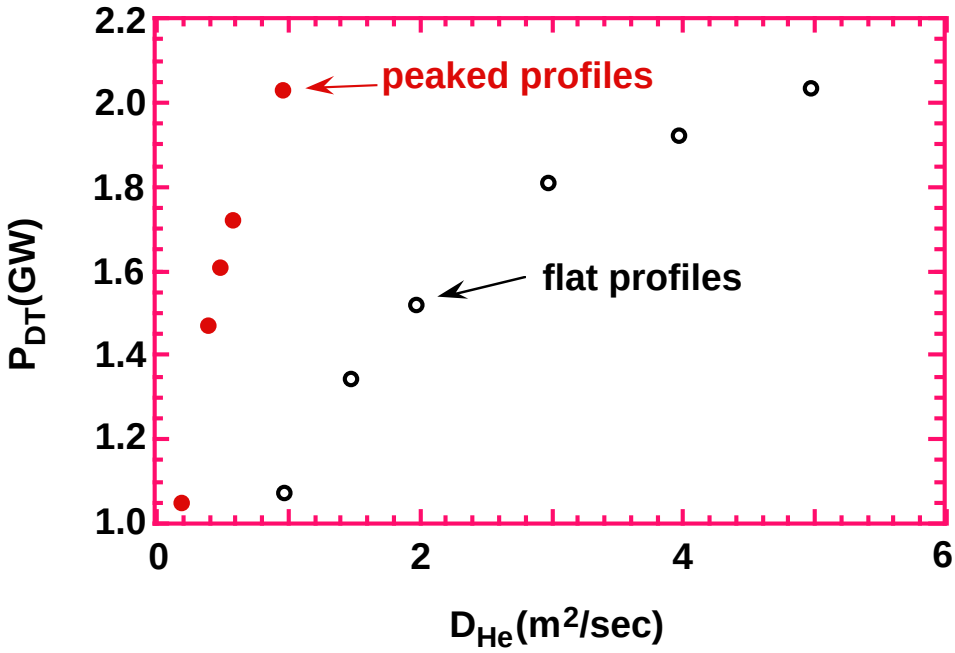

Fig. 18-d

Fusion Power

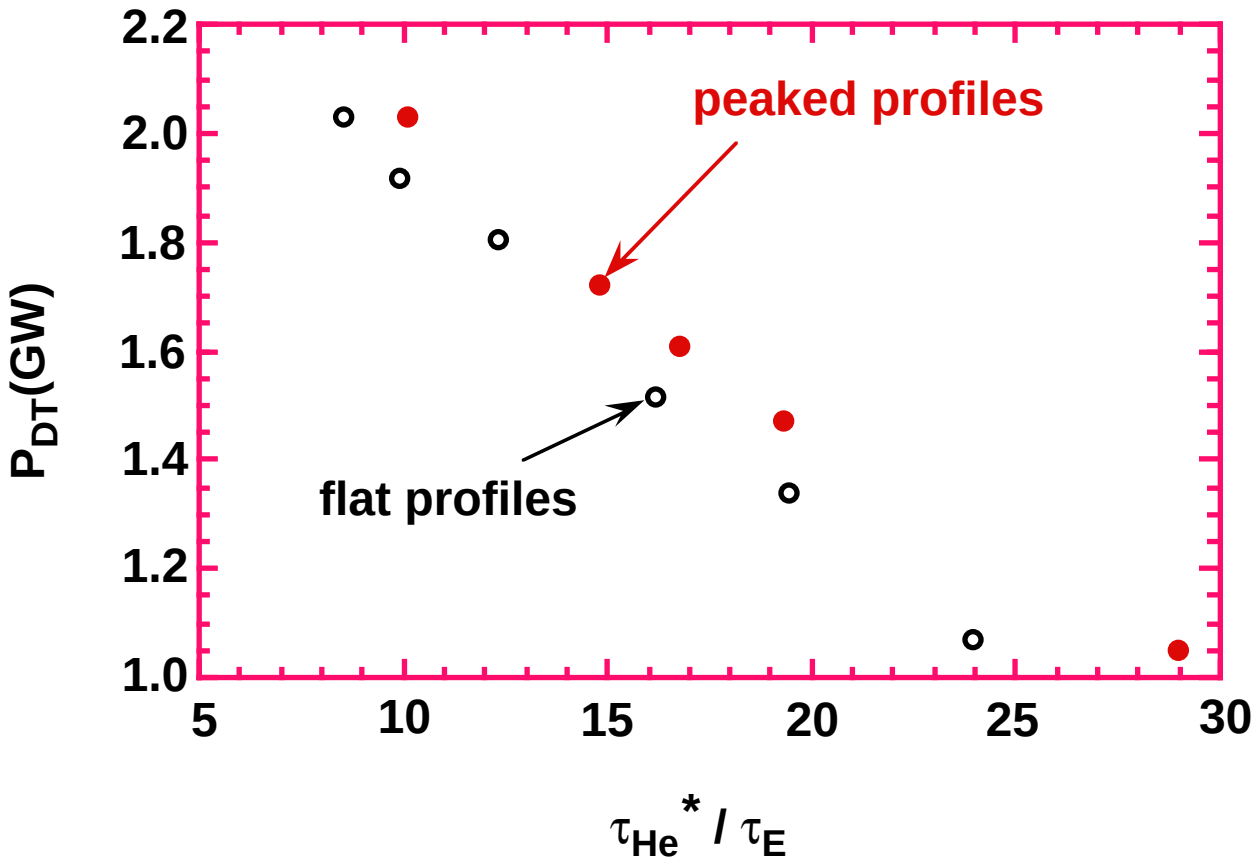

Fig. 19